EFFECTS OF WIDTH OF FAULT FRACTURE ZONE ON FAILURE MECHANISMS OF MOUNTAIN TUNNELS CROSSING ACTIVE STRIKE-SLIP FAULTS

Z. Wang(1), Z. Zhong(2), M. Zhao(3), H. Wang(4), X. Du(5)

(1) *Ph.D. Student, Beijing University of Technology, wangzhenSKG@126.com*
(2) *Associate Professor, Beijing University of Technology, zilanzhong@bjut.edu.cn*
(3) *Professor, Beijing University of Technology, zhaomi@bjut.edu.cn*
(4) *Ph.D. Student, Beijing University of Technology, whr39255@163.com*
(5) *Professor, Beijing University of Technology, duxiuli5@126.com*

Abstract

The active fault zone is an unfavorable geological problem often encountered in the design and construction of long underground engineering structures. It is common to see that mountain tunnels cross different fault fracture zones in seismic active regions. In the past, it was generally believed that mountain tunnels would suffer less seismic damage than aboveground structures and shallow buried urban tunnels due to their large buried depth in rock strata. However, recent post-earthquake investigations on the seismic damage of tunnels reveal that many mountain tunnels suffered severe structural damage in the forms of longitudinal and circumferential lining cracks, concrete spalling, reinforcement yielding and water leakage, which primarily concentrated in the fault fracture zones. The damage of mountain tunnels caused by fault ruptures are usually severe and destructive, which is a critical concern in engineering practice. This paper primarily focuses on the numerical investigations of the effects of width of fault fracture zone on failure mechanism of mountain tunnels crossing active strike-slip faults. In this study, the Xianglu mountain tunnel of the water diversion project in the central Yunnan province, China, is used as the engineering background. A three-dimensional numerical model of the tunnel is established using the finite element method in this study. An excavation simulation scheme, which assumed that the tunnel is excavated instantaneously from one side of the rock mass to the other side, is adopted in this paper for the excavation process to address the initial stress state in the tunnel. The fault displacement is subsequently applied in a quasi-static manner to the moving block of the rock mass. The ovalization coefficients are adopted to estimate the structural damage of the tunnel. Different deformation patterns and failure mechanisms of tunnels under the strike-slip faulting based on the numerical results are summarized in this paper. The results indicated that cross-sectional ovalization of the tunnel at the central plane of the fault fracture zone decreases first and remain almost constant as the width of the fault fracture zone increases. The fault fracture zone is stretched under fault movement and also deforms vertically under gravity, causing the tensile and compressive damage to the vault and the bottom of tunnel respectively. Typical failure mechanisms of tunnels by faulting mainly include shear failure, horizontal bending failure and vertical bending failure. Overall, the width of fault fracture zone has significant influence on the failure modes of the tunnel and should be considered in the design of tunnel crossing active faults.

Keywords: Mountain tunnels; Fault fracture zone; Strike-slip faults; Damage pattern; Deformation response

1. Introduction

The geological characteristics of active fault zones including low strength, fragility non-homogeneity, and high water permeability are potential threats to the structural integrity and safety of mountain tunnels. In the past, it was generally believed that mountain tunnels would suffer less seismic damage than aboveground structures and shallow buried urban tunnels due to their large buried depths in the rock strata. However, recent post-earthquake investigations revealed that many mountain tunnels suffered severe structural damage (Lai et al., 2017; Roy and Sarkar, 2017; Sharma and Judd, 1991). For instance, based on the previous post-earthquake survey reports, the aqueduct of the Shihgang dam was completely destroyed by lateral shear forces at 180 m downstream from the inlet because of the fault movement in the 1999 Chi-Chi earthquake (Wang et al., 2001). During the 2008 Wenchuan earthquake, numerous tunnels suffered lateral shear failure near the epicenter and the fault fracture zone. A typical lining dislocations up to approximately 30 cm occurred in the Baiyunding tunnel in the dislocated fault fracture zone (Gao, et al., 2009).

Both numerical and experimental studies have been performed by many researchers to investigate the seismic response of the long-span lifeline crossing active faults and proposed useful suggestions for engineering practice. Related research work mainly focused on the following aspects: (1) deformations of cover layers caused by the bedrock offset and propagation characteristics of fault ruptures (Anastasopoulos et al., 2007; Bransby et al., 2008; Chang et al., 2015); (2) investigation of mechanical behavior and failure mechanism of tunnels and pipelines subjected to fault rupture with specific focus on the effects of fault dip angle, intersection angle between fault and buried structure, and fault types (Erami et al., 2015; Jalali et al., 2016; Liu et al., 2015; Vazouras et al., 2017); (3) dynamic response characteristics and seismic damage evolution of buried structures crossing the fault fracture zone (Huang et al., 2017; Yang et al., 2013); and (4) seismic design and countermeasures of buried structures crossing the fault fracture zone (Shahidi and Vafaeian, 2005; Xin et al., 2014).

Overall, most of the researchers neglected the effect of width of the fault fracture zone on the seismic response of underground structures in their studies and simply assumed the fault to be a zero-thickness interface. However, in engineering practice, the faults lie at the construction paths of mountain tunnels are usually in the forms of fracture zones with different widths, ranging from a few centimeters to hundreds of meters. For instance, in the 2008 Wenchuan earthquake, five of the six tunnels traversing fault fracture zone with widths ranging from 0.5 m to 64 m experienced different levels of seismic damage caused by fault movement. The Youyi tunnel, the Longxi tunnel and the Jiujiaya tunnel cross the fault fracture zones with width of 0.5 m, 10 m and 64 m, respectively. Post-earthquake indicate that the seismic damage in the Longxi tunnel and the Jiujiaya tunnel were much serious than the Youyi tunnel (Cui et al., 2013). Hashash et al. (2001) also pointed out that seismic design of tunnels crossing active faults should consider both the magnitude of fault displacement and the width of the fault fracture zone over which that displacement is distributed. Therefore, the width of fault fracture zone, which plays a prominent role in the tunnel's behavior and damage evolution under fault movement, is a critical parameter to be considered in the seismic design of mountain tunnels.

In this paper, a three-dimensional (3D) numerical model of a mountain tunnel crossing an active strike-slip fault is established based on the Xianglu mountain tunnel. The effects of fault fracture zone with different widths on the longitudinal and cross-sectional deformations, the stress distributions and the failure mechanism of the tunnel are presented and discussed in this study. Furthermore, different failure modes of tunnels subjected to strike-slip fault displacement with consideration of the widths of fault fracture zone are summarized in this paper in order to provide technical supports for seismic design and rehabilitation of mountain tunnels crossing active faults.

2. Numerical modeling

2.1 Engineering background

Fig. 1 shows the geological profile of the Lijiang-Jianchan fault fracture zone along the path of the Xianglu mountain tunnel. The Xianglu mountain tunnel crossing Faults F11-2, F11-3 and F11-4, and the angles between the line axis and the faults is about 46°~88°. According to the geological survey, there is a weak rock mass belt with a length of about 1340m between F11-3 and F11-4, which is referred to herein as a "fracture zone". In this paper, only the portions of the tunnel between Faults F11-3~F11-4 is selected as the engineering background for the numerical study.

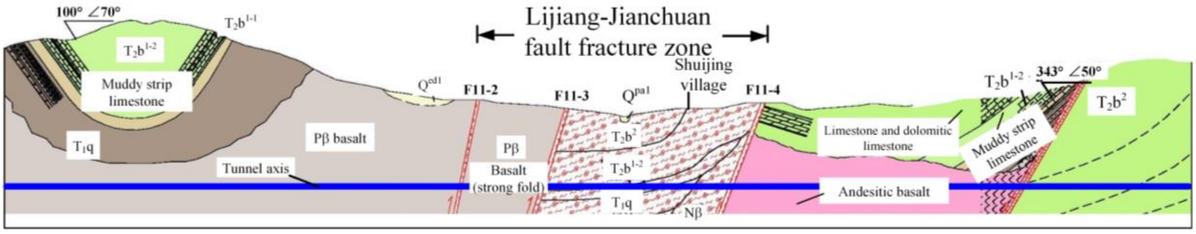

Fig. 1. Geological profile of Xianglu mountain tunnel

2.2 Numerical modeling

Fig. 2 shows the mesh of the numerical model of the fault-tunnel interaction system. The numerical model has an overall dimension of 100 m × 300 m × 400 m, and the burial depth of the tunnel is 100 m. The water tunnel has an outer and inner diameters of 9.4 m and 8.0 m respectively. Sensitivity analysis shows that the boundary effects on the response of the tunnel is insignificant. The fault along the path of Xianglu mountain tunnel is simplified as a left-lateral strike-slip fault with different widths in the numerical analysis. The fault dip angle and the angle between the tunnel axis and the fault direction are assumed to be 90°.

The numerical model can be divided in to three blocks by the interfaces between the integral rock mass and the fault fracture zone, which are the fixed block, the fault fracture zone and the moving block. The fixed block and the moving block are of the same dimensions. Eight-node reduced-integration brick elements (C3D8R) are used to simulate the integral rock mass and the fault fracture zone. Eight-node brick elements (C3D8) are employed for modeling tunnels. The sizes of meshing are different in different regions of the model. The mesh in the fault fracture zone is much finer than that in the integral rock mass. The mesh of the integral rock mass far from the fault fracture zone is much coarser, as shown in Fig. 2(a). The mesh size on the cross section (x-y plane) of the numerical model is smaller in the region within 20 m from the tunnel. The mesh size of the rock mass of ground far from the tunnel on the cross section of the numerical model is coarser, as shown in Fig. 2(b). Furthermore, a total of 48 solid elements around the cylinder circumference are adopted in the tunnel, as shown in Fig. 2(c).

The primary lining is tied to the surrounding rock mass in the numerical analysis. The interaction between the primary lining and the secondary lining is modelled by the friction contact. The friction coefficient in the tangential direction is assumed to be 0.4. The mechanical behavior of the rock masses is described by the elastic-perfectly plastic Mohr-Coulomb model, which is characterized by the cohesion c, the friction angle ϕ, the elastic modulus E and the Poisson's ratio ν and the dilation angle ψ. The concrete damaged plasticity model is used to simulate the tunnel. The geomechanical properties used for 3D numerical model are shown in Table 1.

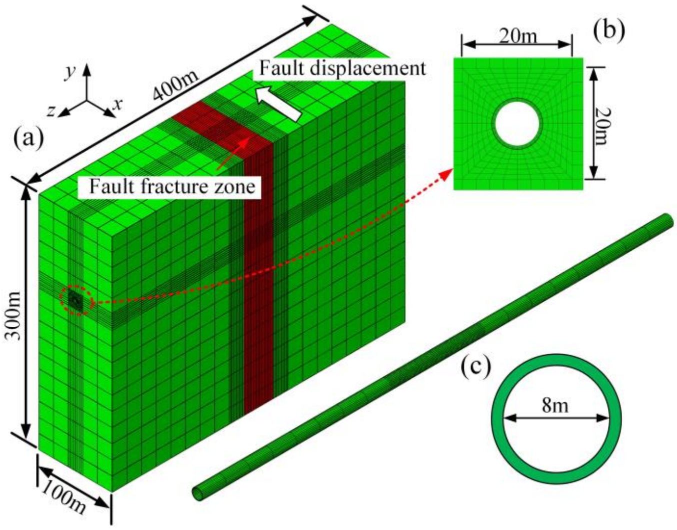

Fig. 2. Finite element model: (a) mesh of rock mass and fault fracture zone; (b) mesh of surrounding rock in *x*-*y* plane near tunnel; (c) mesh of tunnel

Table 1. Physic and mechanical properties of materials

Type	Grade	Density (kg m^{-3})	Elastic modulus (GPa)	Poisson's ratio	Internal frication angle (°)	Cohesion (MPa)
Integral rock mass	III	2930	7.5	0.28	45	1.1
Fault fracture zone	IV	2100	1.5	0.33	29	0.15
Primary lining	–	2500	28	0.2	–	–
Secondary lining	–	2500	30	0.2	–	–

Note: The grade of rocks is adopted from the Chinese Code for Guidelines for Design of Highway Tunnel (JTG/T D70-2010), and higher grades indicate poorer rock qualities.

In this paper, the excavation process is considered to simulate a more realistic initial stress state of the tunnel before fault movement. A single-step excavation scheme is adopted for the excavation process (Yoo., 2002). The procedure of this method includes removal of all the rock masses inside the tunnel completely at one time, and application of the reverse nodal forces at the excavation surface to maintain the force equilibrium, and finally gradually release of the nodal forces to simulate the stress release process during excavation. The schematic diagram of the tunnel excavation process is shown in Fig. 3.

According to the geological investigation report of Xianglu mountain tunnel, the expected relative horizontal fault movement is approximately 0.5 m during the service life of the tunnel (100 years). Therefore, in this paper, a relative fault displacement of 0.5 m between the fixed and the moving blocks is applied to the numerical model after the tunnel excavation, using the pseudo-static scheme.

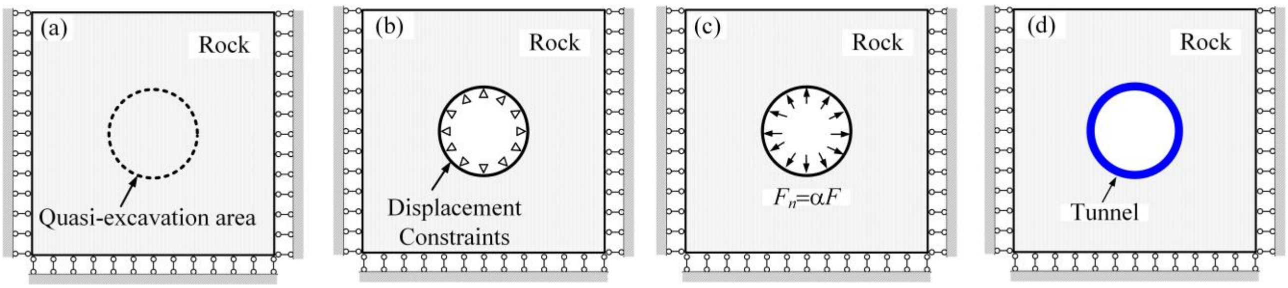

Fig. 3. Schematic of tunnel excavation process: (a) application of gravity; (b) displacement constraint to tunnel-rock interface; (c) application and release of nodal reaction forces to tunnel-rock interface; (d) introduction of tunnel structure

3. Numerical results

In order to investigate the influence of widths of fault fracture zone on tunnel structural response and failure modes, a total of six numerical models were built in ABAQUS with the width of the fault fracture zone varying from 1/4*D* (2 m) to 5*D* (40 m), where, D = 8 m is the tunnel inner diameter. Since the structural damage of the secondary lining will directly lead to the loss of function of the water tunnel, this study primarily focuses on the structural response of the secondary lining as presented in the following sections.

3.1 Displacement of tunnel crown

It is found from the numerical results that the lateral displacement responses of the tunnel caused by fault displacement is roughly the same at the crown, shoulder and invert of the tunnel. Therefore, only the lateral displacements of the crown of the tunnel lining are presented in this section for brevity. Fig. 4 shows the peak lateral displacement at the crown at a peak fault displacement Δ of 0.5 m, where the abscissa represents the distance from the central plane of the fault fracture zone. It can be seen that for all the six models, the lateral displacement of the tunnel increases from zero in the fixed block of rock mass to 0.5 m in the moving block of rock mass along the faulting direction. All the curves of the lateral displacement show an anti-symmetric pattern and intersect at the center of the fault fracture zone. As the width of the fault increases, the shape of the lateral displacement gradually changes from Z-shape to S-shape. Moreover, when the width of the fault fracture zone is less than or equal to 1*D*, each curve has two inflection points. The steep slopes of the curves between the two inflection points indicate significant lateral deformation of the tunnel in this region. When the width of the fault fracture zone exceeds 1*D*, each curve has four inflection points. The deformation of the tunnel mainly concentrates at the interface between the rock mass and the fault fracture zone. While, in the central region of the fault fracture zone, the slope of the curve is much flatter indicating smaller lateral deformation of the tunnel in this region.

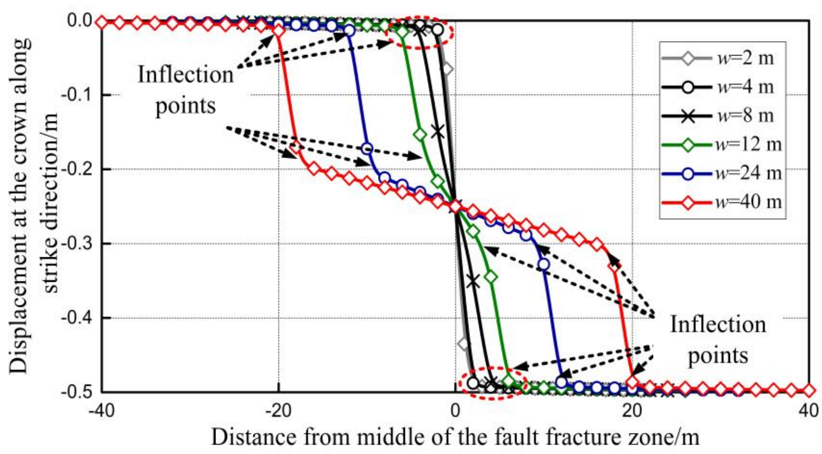

Fig. 4. Lateral displacement of tunnel crown along faulting direction

Fig. 5 shows the vertical displacement at the tunnel crown of the peak fault displacement Δ of 0.5 m. When the width of the fault fracture zone is less than or equal to 1/2*D*, the magnitude of fault displacement is distributed in the fault fracture zone with a small width, leading to high shear stress concentration at the tunnel and surrounding rock in the fault fracture zone. Local shear failure at the vicinity of the fault fracture zone leads to the vertical displacement at the tunnel crown. Tensile forces start to contribute more to the failure of the surrounding rock close to the tunnel, as the width of the fault fracture zone increases. For those cases, the damaged rock mass in the fault fracture zone firstly collapses under gravity, and subsequently induces large vertical displacement to the portions of the tunnel close to the two interfaces between the rock masses and the fault fracture zone.

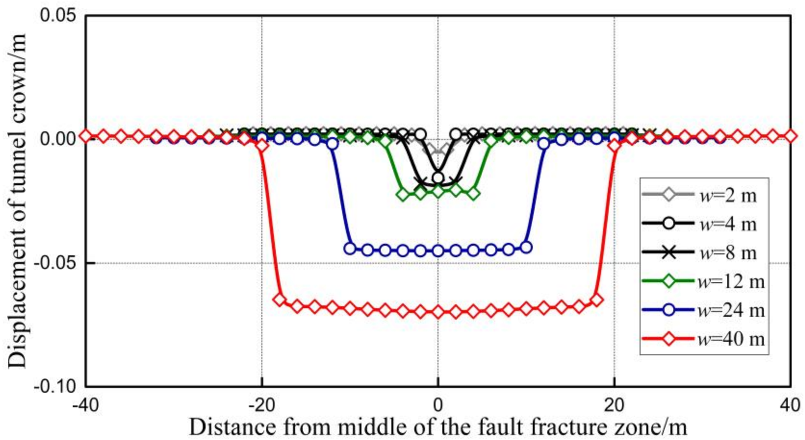

Fig. 5. Vertical displacement at tunnel crown along faulting direction

3.2 Distortion of tunnel cross-section

The cross-sectional distortion of the tunnel is one of the most important measures to characterize the structural damage of the tunnel. Two main reasons contribute to the cross-sectional distortion of the tunnel: (1) the stress release of the rock mass during the excavation causes the cross section of the tunnel to change from a circle to a horizontal ellipse; (2) the irregular distortion of the tunnel cross section caused by the fault displacement. The cross-sectional distortion is divided into two modes in this paper, from a circle to a vertical ellipse or a transverse ellipse, as shown in Fig. 6. Ovalization is a simple and efficient measure to estimate the cross-sectional distortion of a circular tunnel. Two non-dimensional 'ovalization coefficients', f_h and f_v, defined in Eq. 1, are adopted in this section to quantify the ovalization of the cross section along the horizontal and vertical axes, namely Axis 1 and Axis 2, respectively, as shown in Fig. 6.

$$\begin{cases} f_h = \Delta D_h / D \\ f_v = \Delta D_v / D \end{cases} \tag{1}$$

where, ΔD_h and ΔD_v are the changes of cross-sectional diameter in the horizontal and vertical directions, respectively. Positive and negative values indicate expansion and contraction of the cross sections, respectively.

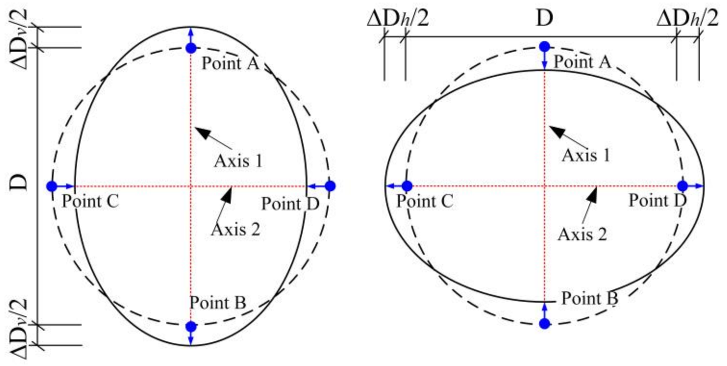

Fig. 6. Schematic of ovalization of tunnel cross-section in horizontal and vertical directions

Fig. 7(a) shows the cross-sectional ovalization of the tunnel at the central plane of the fault fracture zone, as highlighted by the red plane at the peak fault displacement of 0.5 m. It is found that, when the width of the fault fracture zone is less than 3*D*, $|\Delta D_v/D|$ and $|\Delta D_h/D|$ decrease with the increase of the width of the fault fracture zone. $|\Delta D_v/D|$ reduces from 16.62‰ to 3.84‰ and $|\Delta D_h/D|$ reduces from 22.62‰ to 1.50‰. It should be noted that both $\Delta D_v/D$ and $\Delta D_h/D$ are negative, indicating that the tunnel cross section is contracting in both the horizontal and vertical directions. When the width of the fault fracture zone, *w*, is greater than or equal to 3D, $|\Delta D_v/D|$ and $|\Delta D_h/D|$ remain almost constant as the width of the fault fracture zone increases. The cross-sectional ovalization of the tunnel remains at a low level (less than 1% in both directions) for the cases of *w* larger than 3*D*, indicating that the fault width has insignificant effects on the cross-sectional deformation of the tunnel close to the central plane of the fault fracture zone.

Fig. 7(b) presents the cross-sectional ovalization of the tunnel at the interface between the rock mass and the fault fracture zone. It can be seen from the numerical results that both $|\Delta D_v/D|$ and $|\Delta D_h/D|$ decrease first and then increase with the increase of *w*. For the case of $w = D$, the $|\Delta D_v/D|$ and $|\Delta D_h/D|$ reach their minimum values of 6.55‰ and 6.42‰ respectively. Again, negative values of $\Delta D_v/D$ and $\Delta D_h/D$ for all the numerical case studies with different *w* indicate that the tunnel cross section is primarily under compression in both the horizontal and vertical directions.

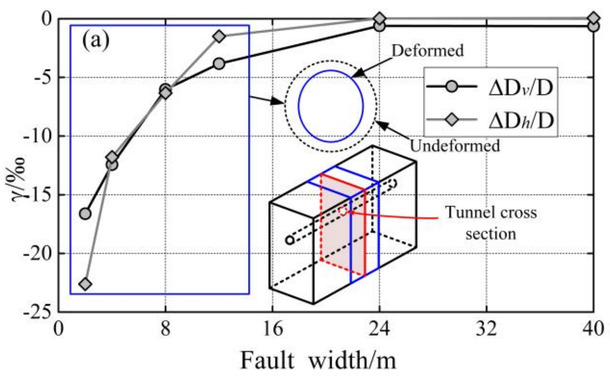

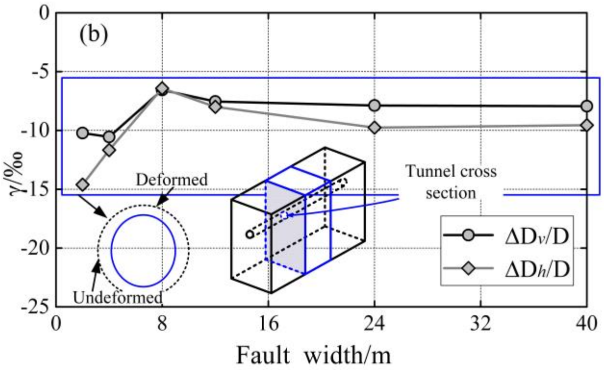

Fig. 7. Effects of width of fault fracture zone on ovalizon of tunnel cross section: (a) at central plane of the fault fracture zone; (b) at interfaces between integral rock masses and fault fracture zone

4. Failure modes of mountain tunnels

Under the strike-slip fault displacement, the tunnel structure is subjected to a complicated loading combination of stretching, compression, bending and shearing. Based on this numerical study, the influence of the strike-slip fault on the tunnel structure can be mainly attributed to the following two aspects: (1) the relative movement between the rock mass and the fault fracture zone; (2) the damaged fault fracture zone collapses under gravity, which causes the relative movement between the rock mass and the fault fracture zone in the vertical direction. In this section, the following three typical failure modes of the tunnel crossing a strike-slip fault are identified based on the numerical study.

4.1 Shear failure

In this failure mode, the tunnel lining close to the interface between the integral rock masses and the fault fracture zone is directly sheared apart, as shown in Fig. 8(a). Fig. 8(b) shows a typical transverse shear failure of the Baiyunding tunnel in the Wenchuan earthquake, where the secondary lining dislocation reached approximately 30 cm. When the fault displacement is large enough, structural damage to the tunnel further develops from local lining dislocation to completely lining collapse. Fig. 8(c) shows a typical secondary lining collapse of the Jiujiaya tunnel in the Wenchuan earthquake.

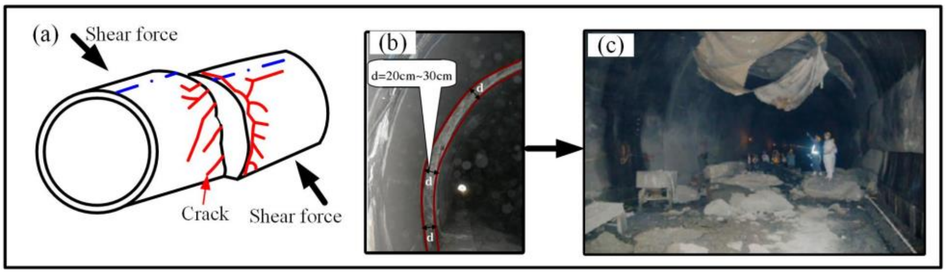

Fig. 8. Shear failure of tunnels under fault displacement (Shen et al., 2014)

4.2 Horizontal bending failure

For this failure mode, significant cross-sectional bending moment develops in the tunnel under the strike-slip fault displacement. The bending moment causes tensile and compressive damage to the tunnel waists near the two interfaces between the integral rock masses and the fault fracture zone as shown in Fig. 9(a). Fig. 9(b) shows a typical compression damage at the tunnel waist of the secondary lining of the Longxi tunnel caused by horizontal bending in the Wenchuan earthquake

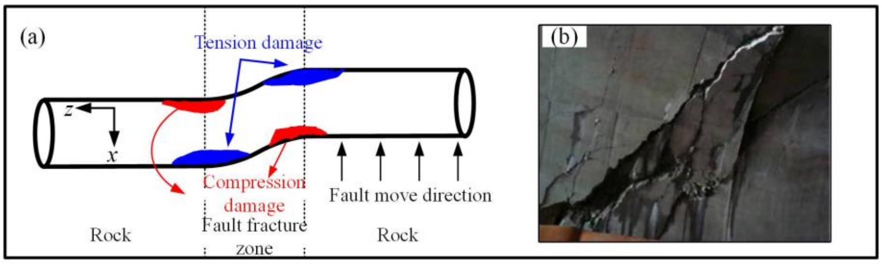

Fig. 9. Bending damage of tunnel the movement of the strike-slip fault (Plane view)

4.3 Vertical bending and shear failure

In this failure mode, the fault fracture zone is stretched and sheared under the movement of the strike-slip fault and the fragile rock masses in the fault fracture zone collapse under gravity, causing relative displacements between the fault fracture zone and the integral rock masses. The overburden pressure formed at the tunnel crown leading to compressive-shear or bending failure at the crown, shoulder and invert of the tunnel. Finally, a circumferential damage zone in the tunnel lining forms close to the interface between the integral rock mass and the fault fracture zone leading to the failure of the tunnel, as shown in Fig. 10.

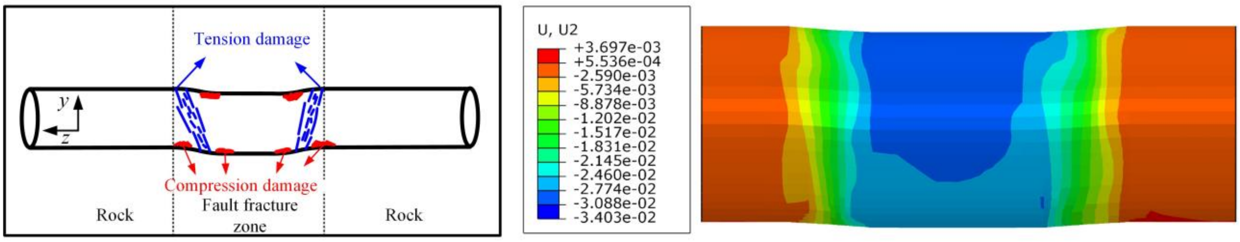

Fig. 10. Vertical bending and shear damage of tunnel under movement of strike-slip fault (Side view)

5. Summary and conclusions

In this paper, the structural response and damage mechanism of tunnels under strike-slip faulting are studied based on the Xianglu mountain tunnel of the water diversion project in the central Yunnan province, China. In the numerical study, the influence of the initial stress in the tunnel is considered by introducing excavation simulation of the tunnel to the analysis. The fault displacement is subsequently applied after tunnel excavation to investigate the effects of the width of the fault fracture zone on the failure modes of the tunnel. The structural response of the tunnel in terms of lateral and vertical displacement, cross-sectional distortion are discussed under different widths of the fault fracture zone and fault displacements. The following conclusions are drawn from this study:

(1) With the increase of the width of the fault fracture zone, the lateral displacement of the tunnel along its axis gradually changes from Z-shape to S-shape. When the width of the fault fracture zone exceeds 1.5*D*, the lateral displacement of the tunnel is mainly concentrated at the two interfaces between the integral rock masses and the fault fracture zone.

(2) For the cases of fault fracture width larger than 1.5*D*, the fault fracture zone is stretched and sheared under faulting. The fragile rock mass in the fault fracture zone collapses under gravity, leading to the vertical displacement of the tunnel. Large vertical displacement of the tunnel mainly occurs near the interfaces between the integral rock mass and the fault fracture zone.

(3) The cross-sectional ovalization of the tunnel remains at a low level for the cases of fault width larger than 3*D*, indicating that the fault width has insignificant effects on the cross-sectional deformation of the tunnel close to the central plane of the fault fracture zone.

(4) The width of fault fracture zone will significantly affect the failure mode and cross-sectional distortion of the tunnel.

6. References

[1] Anastasopoulos I, Gazetas G, Bransby MF, Davies MCR, Nahas AE (2007): Fault rupture propagation through sand: finite-element analysis and validation through centrifuge experiments. *Journal of Geotechnical and Geoenvironmental Engineering*, 133 (8), 943-958.

[2] Bransby MF, Davies MCR, Nahas AE (2008): Centrifuge modelling of normal fault-foundation interaction. *Bulletin of Earthquake Engineering*, 6, 585-605.

[3] Chang YY, Lee CJ, Huang WC, Hung WY, Huang WJ, Lin ML, Chen YH (2015): Evolution of the surface deformation profile and subsurface distortion zone during reverse faulting through overburden sand. *Engineering Geology*, 184, 52-70.

[4] Cui GY, Wang MN, Yu L, Lin GJ (2013): Study on the characteristics and mechanism of seismic damage for tunnel structures on fault rupture zone in Wenchuan seismic disastrous area. *China Civil Engineering Journal*, 46 (11): 122-127 (in Chinese).

[5] Erami MH, Miyajima M, Kaneko S, Toshima T, Kishi S (2015): Pipe-soil interaction for segmented buried pipelines subjected to dip faults. Earthquake Engineering and Structural Dynamics, 44 (3), 403-417.

[6] Gao, B, Wang, ZZ, Yuan, S, Shen YS (2009): Lessons learnt from damage of highway tunnels in Wenchuan earthquake. *Journal of Southwest Jiaotong University*. 44 (3), 336–341 (in Chinese).

[7] Hashash YMA, Hook JJ, Schmidt B, Yao JI (2001): Seismic design and analysis of underground structures. *Tunnelling and Underground Space Technology*, 16, 247-293.

[8] Huang JQ, Zhao M, Du XL (2017): Non-linear seismic responses of tunnels within normal fault ground under obliquely incident P waves. *Tunnelling and Underground Space Technology*, 61, 26-39.

[9] Jalali HH, Rofooei FR, Attari NKA, Samadian M (2016): Experimental and finite element study of the reverse faulting effects on buried continuous steel gas pipelines. *Soil Dynamics and Earthquake Engineering*, 86, 1-14.

[10] Lai JX, He SY, Qiu JL, Chen JX, Wang LX, Wang K, Wang JB (2017): Characteristics of seismic disasters and aseismic measures of tunnels in Wenchuan earthquake. *Environmental Earth Sciences*, 76 (2), 76-94.

[11] Liu XZ, Li XF, Sang YL, Lin LL (2015): Experimental study on normal fault rupture propagation in loose strata and its impact on mountain tunnels. *Tunnelling and Underground Space Technology*, 49, 417-425.

[12] Roy N, Sarkar R (2017): A review of seismic damage of mountain tunnels and probable failure mechanisms. *Geotechnical and Geological Engineering*, 35, 1-28.

[13] Shahidi AR, Vafaeian M (2005): Analysis of longitudinal profile of the tunnels in the active faulted zone and designing the flexible lining (for Koohrang-III tunnel). *Tunnelling and Underground Space Technology*, 20 (3), 213-221.

[14] Sharma S, Judd WR (1991): Underground opening damage from earthquakes. *Engineering Geology*, 30, 263-276.

[15] Shen YS, Gao B, Yang XM, Tao SJ (2014): Seismic damage mechanism and dynamic deformation characteristic analysis of mountain tunnel after Wenchuan earthquake. *Engineering Geology*, 180, 85-98.

[16] Vazouras P, Karamanos SA (2017): Structural behavior of buried pipe bends and their effect on pipeline response in fault crossing areas. *Bulletin of Earthquake Engineering*, (2), 1-26.

[17] Wang, WL, Wang, TT, Su, JJ, Lin CH, Seng CR, Huang TH (2001): Assessment of damage in mountain tunnels due to the Taiwan Chi-Chi Earthquake. *Tunnelling and Underground Space Technology*, 16 (3), 133–150.

[18] Xin CL, Gao B, Zhou JM, Sheng YS (2014): Shaking table tests of conventional anti-seismic and damping measures on fault-crossing tunnels. *Chinese Journal of Rock Mechanics and Engineering*, 33 (10), 2047-2055(in Chinese).

[19] Yang ZH, Lan HX, Zhang YS, Gao X, Li LP (2013): Nonlinear dynamic failure process of tunnel-fault system in response to strong seismic event. *Journal of Asian Earth Sciences*, 64, 125-135.

[20] Yoo C (2002): Finite-element analysis of tunnel face reinforced by longitudinal pipes. *Computers and Geotechnics*, 29 (1), 73-94.

